SETI Antonio Feed Thermal Analysis

Prepared By:	Fiona Hillier Senior Thermal Engineer	Signature and Date:	Digitally signed by Fiona Hillier Date: 2020.06.03 10:40:03 +01'00'
Checked By:	Bryan Shaughnessy Thermal Group Lead	Signature and Date:	Digitally signed by Bryan Shaughnessy Date: 2020.06.03 10:50:47 +01'00'
Authorised by:	Bryan Shaughnessy Thermal Group Lead	Signature and Date:	

Change Record

Issue	Date	Section(s) Affected	Description of Change/Change Request Reference/Remarks
1.0	03/06/2020	All	First release

Distribution List

Distribution	Company	Name
x	SETI Institute	Alexander Pollak
x	SETI Institute	Andrew Siemion
x	University of California, Berkeley	Gregory Dalton

TABLE OF CONTENTS

1 Scope

This document presents the thermal analysis of the current design of the Antonio feed and the results of investigations into the following potential thermal design improvements:

- Reducing the emissivity of the feed surface
- Increasing the thermal isolation of the stand-offs between the feed array and the baseplate
- Optimisation of the thermal strap between the cold finger and the feed array
- Increasing the thickness of the feed arms

This document assumes the reader has a familiarity with the feed design, however the CAD model is shown in Figure 1-1 for clarity.

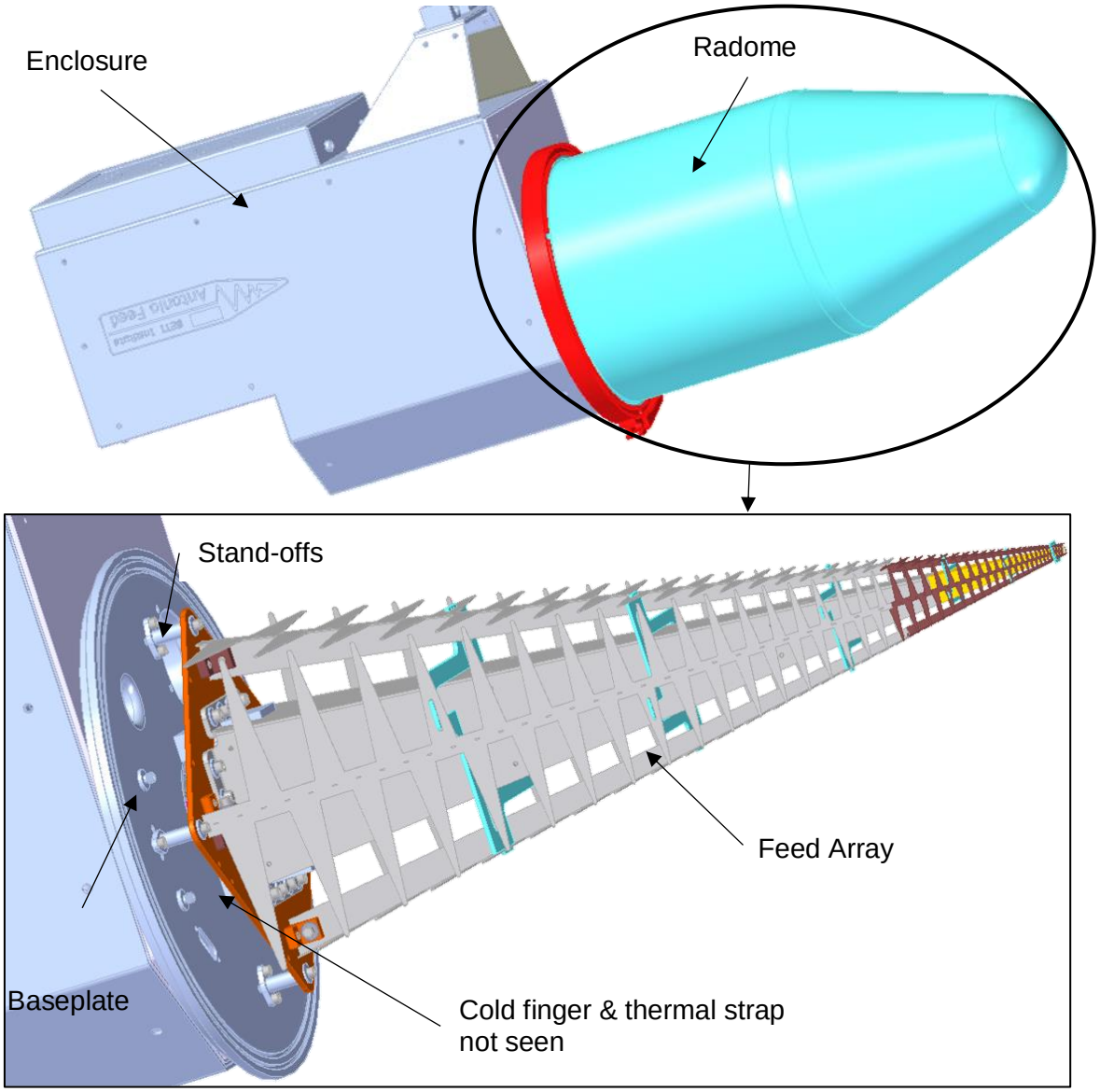

Figure 1-1 Antonio Feed Array CAD Model (RD1)

2 Applicable and reference documents

2.1 Applicable Documents

AD #	Document #	Title
AD1	PO 3530	Feed thermal analysis purchase order

2.2 Reference Documents

The following documents, although not a part of this document, amplify or classify its contents.

RD #	Title
RD1	MEC-30-29-200-B2_ATA_Cooled_Feed_Assy_CAD_19-04-17.zip
RD2	Copy of EPL 30-29-200-B ATA Cooled Feed 5C4 19-04-03 Materials.xlsx
RD3	Spacecraft Thermal Control Handbook Vol 1 – D G Gilmore
RD4	Emissivity and absorptivity measurements on some high-purity metals at low temperatures, D Giulietti and M Lucchesi 1981
RD5	https://www.azom.com/article.aspx?ArticleID=4765 accessed 29/05/2020
RD6	NIST Cryogenic material property database: https://trc.nist.gov/cryogenics/materials/materialproperties.htm accessed 29/05/2020
RD7	Thermal and electrical conductivity measurements of CDA 510 phosphor bronze – J. Tuttle, E. Canavan, and M. DiPirro 2009
RD8	ECSS-E-HB-31-01_Part4A – ECSS Space Engineering Thermal Design Handbook Part 4: Conductive Heat Transfer
RD9	Feed live data: http://antfeeds.setiquest.info/grafana/d/4YbSMt6mz/cryo-health?orgId=1&from=1564676220000&to=1564935420396 accessed 27/05/2020
RD10	GT Cryocooler datasheet - https://www.sunpowerinc.com/-/media/project/ameteksxa/sunpower/ameteksunpower/productdocuments/cryotel-gt-datasheet.pdf?la=en accessed 29/05/2020

3 Terms, definitions and abbreviated terms

Acronym	Definition
AD	Applicable Document
BOM	Bill Of Materials
CAD	Computer Aided Design
GMM	Geometrical Mathematical Model
OFHC	Oxygen Free High Conductivity
RAL	STFC Rutherford Appleton Laboratory
RD	Reference Document
SETI	SETI Institute
TBC	To Be Confirmed
TBD	To Be Determined
TMM	Thermal Mathematical Model

4 Thermal Model Description

The thermal model of the feed has been built and analysed using ESATAN-TMS 2019sp1, a European space industry standard thermal analysis software developed by ITP Engines. The model version described in this document is SETI_TMS_1_0 and is stored on the RAL network drive in the following location: \\space.rl.ac.uk\Projects\Thermal\Thermal_Models\TEG-20-03-SETI_Feed.

The thermal model is a mathematical representation of the heat flows within the assembly. This is achieved by discretising the assembly into nodes, which are areas that can be considered to be isothermal and are assumed to have their mass lumped at the centre of the node. Finite difference method assumptions are then used to solve the resulting partial differential equations of the heat flows between the nodes.

The model of the Antonio feed has been discretised into 1587 nodes, one of which represents the environment. The breakdown of the nodes in each section of the feed is shown in Table 4-1

Part	No. of Nodes
Radome	48
Enclosure Assembly	10
Baseplate	176
Cryocooler*	1
Cryocooler Cold Finger	4
Thermal Strap Assembly	87
Feed Base	24
Feed Central Pyramid	200
Feed Arms	259 (per arm)
Environment*	1

* Held as a boundary temperature

Table 4-1 Node Breakdown

The model can be considered in two sections; the Geometrical Mathematical Model (GMM), and the Thermal Mathematical Model (TMM).

4.1 Geometrical Mathematical Model

The GMM is used to calculate the radiative view factors between the nodes. This is done by creating a geometrical representation of the assembly, including its optical properties. The radiative heat transfer between nodes is then defined by the following equation:

$$Q_{ij} = \sigma \varepsilon_i \alpha_j A_i F_{ij} (T_i^4 - T_j^4)$$

Where:

Q_{ij} = Heat transfer between node i and node j (W)
σ = Stefan-Bolzmann constant ($Wm^{-2}K^{-4}$)
A_i = Area of node i (m^2)
ε_i = IR emissivity of node i
α_j = IR absorptivity of node j
F_{ij} = View factor between node i and node j
T_i = Temperature of node i (K)
T_j = Temperature of node j (K)

The GMM of the Antonio feed is shown in Figure 4-1, including the applied optical properties. The assumed values of the relevant properties are shown in Table 4-2. The geometry has been built from the CAD model in RD1 and BOM in RD2.

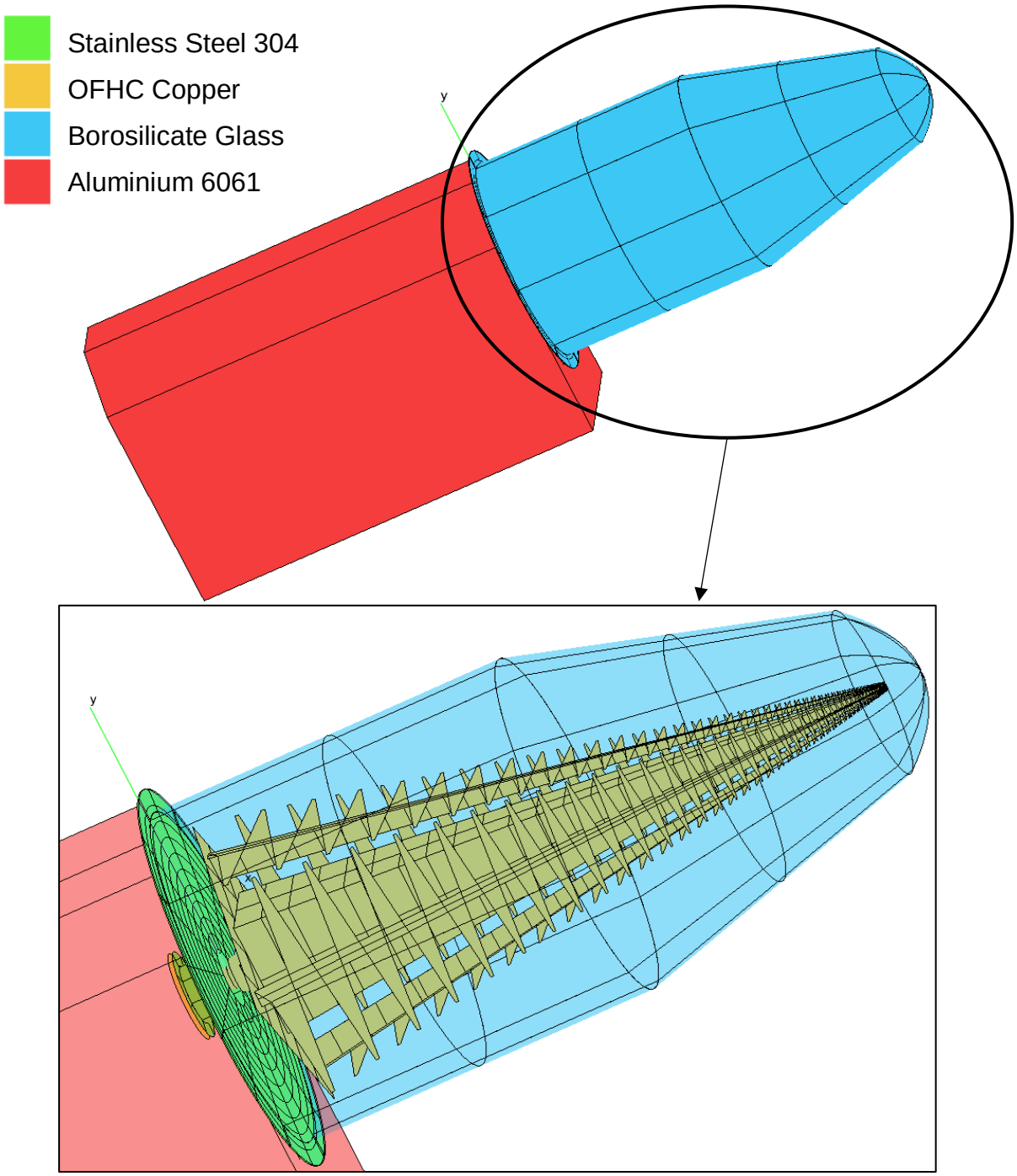

Figure 4-1 Feed GMM & optical properties

Property	Location(s)	Emissivity ε	Transmissivity τ	Reference
Stainless Steel 304	Baseplate	0.14	-	RD3
OFHC Copper	Feed array, cryocooler cold finger, thermal strap	0.13-0.02*	-	RD3, RD4
Borosilicate Glass	Radome	-	0.9	RD5
Aluminium 6061	Enclosure assembly	0.05	-	RD3

* the optical properties assumed for the copper surfaces are varied across this range in the course of the analysis

Table 4-2 Optical Properties

4.2 Thermal Mathematical Model

The TMM is used to calculate the conductive heat transfer between the nodes, combine this with the radiative transfer calculated by the GMM, and solve the resulting partial differential equations using an iterative solver. The solver used for this analysis is ESATANs SOLVIT solution, which calculates a steady state solution by successive point iteration.

The conductive heat transfer between nodes is defined for heat transfer through a solid material as:

$$Q_{ij} = \frac{\lambda A}{x}(T_i - T_j)$$

Where:
Q_{ij} = Heat transfer between node i and node j (W)
λ = Thermal conductivity of material (W/mK)
A = Cross sectional area of heat transfer path (m^2)
x = Length of heat transfer path (m)
T_i = Temperature of node i (K)
T_j = Temperature of node j (K)

And for heat transfer across an interface as:

$$Q_{ij} = Ak(T_i - T_j)$$

Where:
A = Interface area (m^2)
k = Interface conductance (W/m^2K)

The material properties assumed for the conductive calculations are shown in Table 4-3. The material locations have been based on RD2. Part thicknesses and dimensions used for conductive calculations have been taken from RD1.

Property	Location(s)	Thermal Conductivity (W/mK)	Specific Heat Capacity (J/KgK)	Density (Kg/m^3)	Reference
Stainless Steel 304*	Baseplate	8.1	215.3	8000	RD6,RD3
OFHC Copper*	Feed array, Cryocooler cold finger, thermal strap	500.3	205.1	8960	RD6,RD3
Borosilicate Glass	Radome	1.14	830	2230	RD5
Aluminium 6061*	Enclosure assembly	85.6	368.7	2700	RD6,RD3
Ti-6Al-4V*	Stand-offs	3.5			RD6,RD3
Phosphor Bronze	Arm tip links	28.0	-	-	RD7

*Note that the values in the table are shown only at 80 K, however the values used in the model vary with temperature in line with the noted RDs.

Table 4-3 Material Properties

The assumed interface conductances have been taken from RD8, and are dependent on contacting material, contact pressure, and the presence of thermal grease/filler. The relevant graphs from RD8 are shown below. Note that information was not available for interfaces with titanium therefore values for stainless steel were used for the interfaces at either end of the titanium stand offs.

Interface	Location(s)	Graph used
Copper - Copper	Cold finger – thermal strap Thermal strap – feed base Feed base – central pyramid Feed base – arms	Figure 4-2
Copper - Titanium	Feed base – standoff	Figure 4-3
Titanium – stainless steel	Standoff – baseplate	Figure 4-4
Stainless steel – Aluminium	Baseplate - enclosure	Figure 4-5
Glass – Stainless steel	Radome - baseplate	Figure 4-6
Interfaces with thermal grease	-	Figure 4-7

Table 4-4 Interface Assumptions

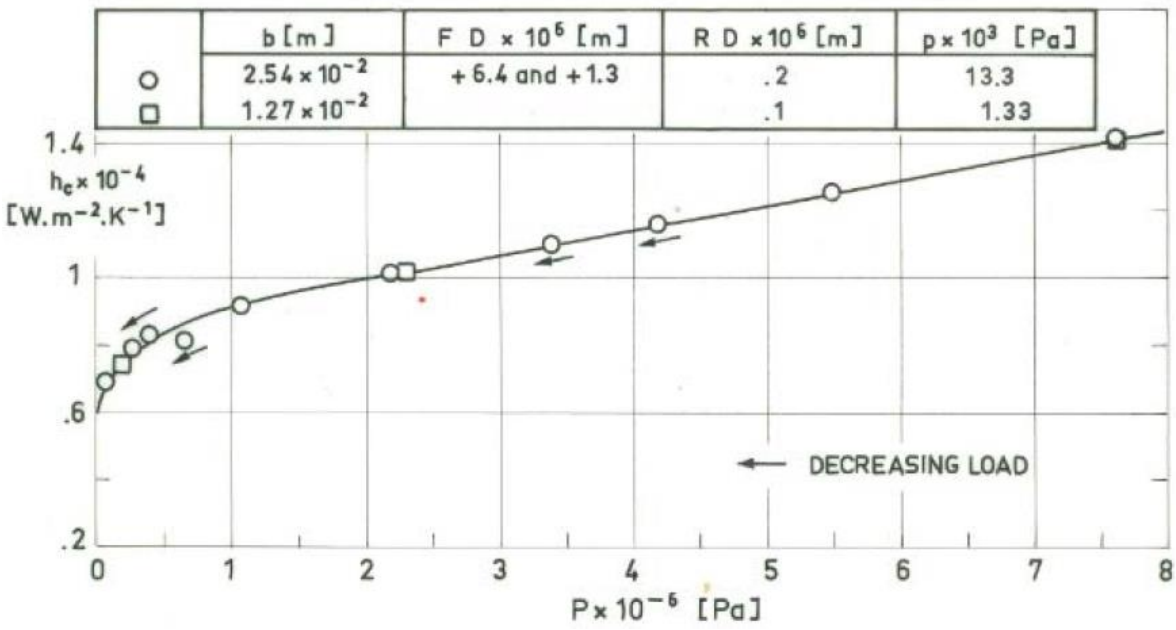

Figure 4-2 Contact conductance between two OFHC copper surfaces from RD8 Figure 5-12

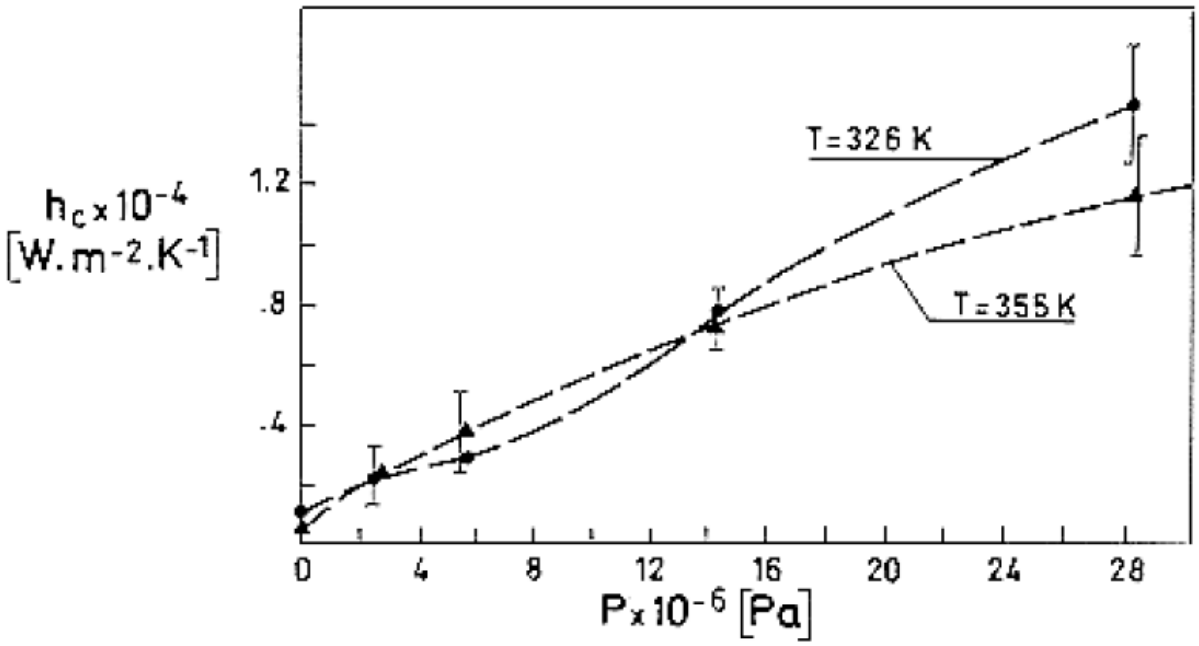

Figure 4-3 Contact conductance between copper and stainless steel from RD8 Figure 5-46

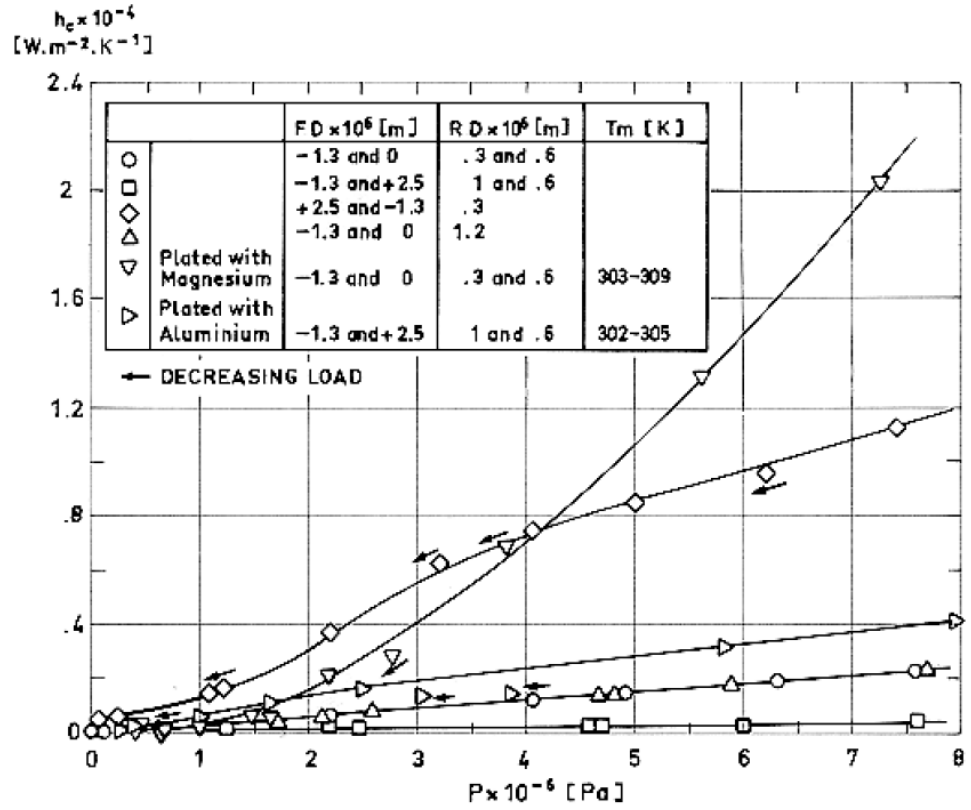

Figure 4-4 Contact conductance between two stainless steel surfaces from RD8 Figure 5-17

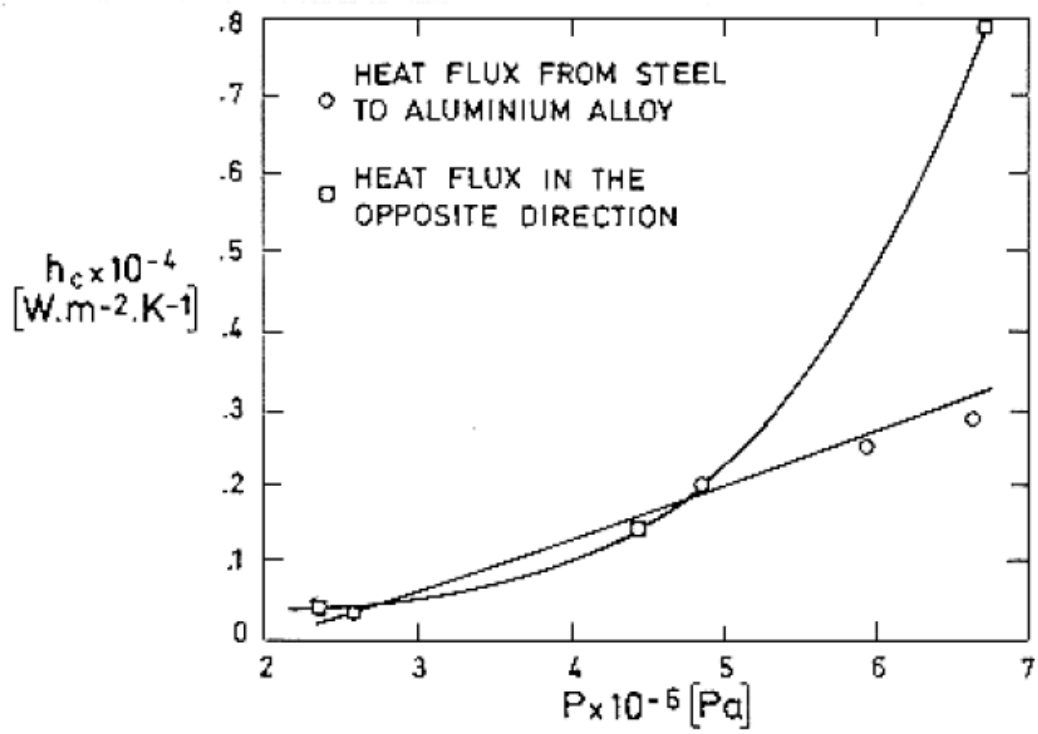

Figure 4-5 Contact conductance between stainless steel and aluminium alloy from RD8 Figure 5-37

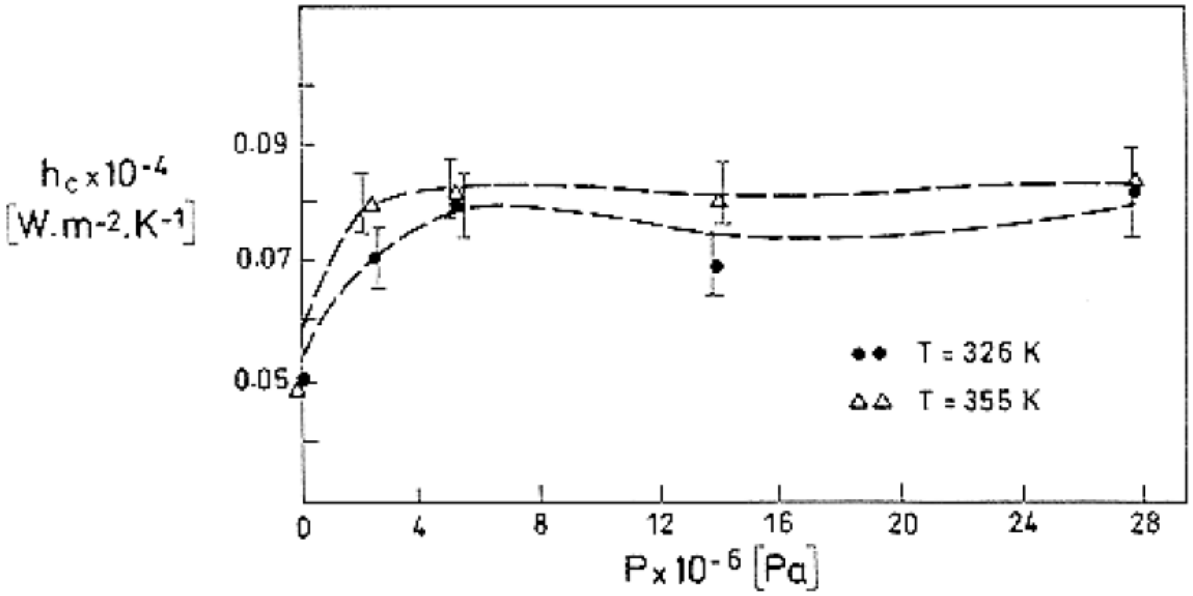

Figure 4-6 Contact conductance between stainless steel and glass epoxy laminate from RD8 Figure 5-57

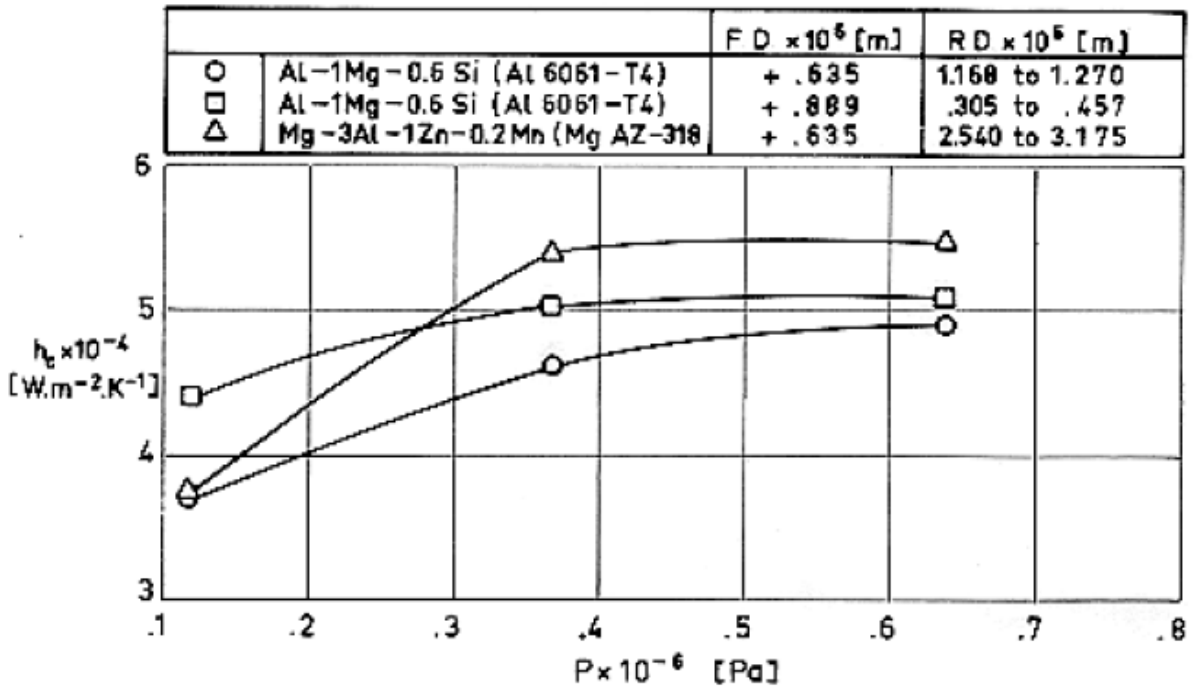

Figure 4-7 Contact conductance between two metallic surfaces with thermal grease from RD8 Figure 5-99

5 Analysis of Current Design

The model described in Section 4 was set up to reflect the current design and situation of the Antonio feed. In order to do this the following parameters were set:

- Cold finger boundary set to 85 K
- Environment boundary set to 298 K
- Emissivity of OFHC Copper set to 0.13 (RD4) to simulate the currently oxidised state of the copper surface

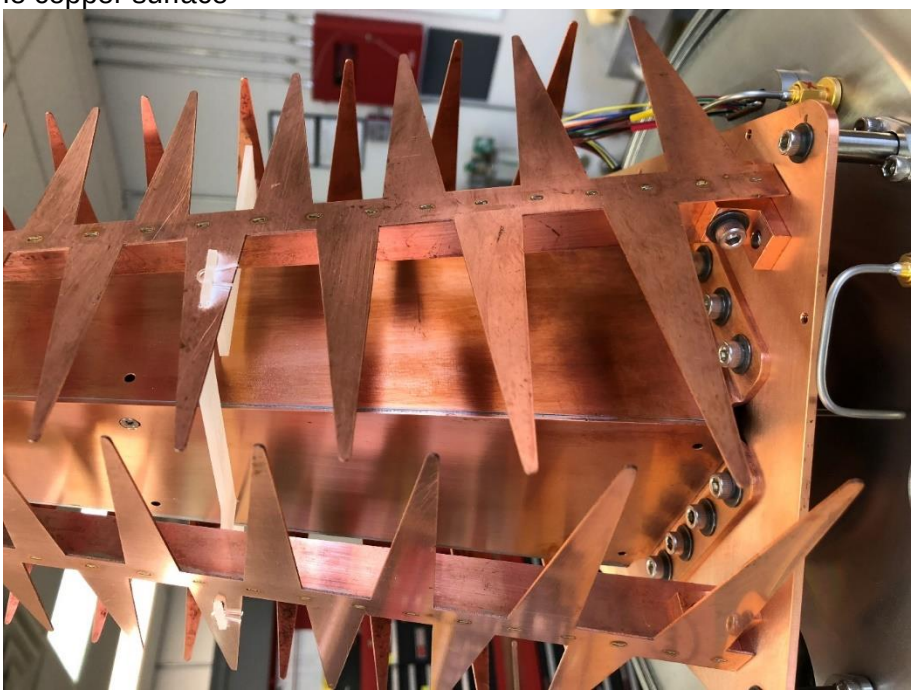

Figure 5-1 Photo of oxidisation on the copper surfaces

The live data from the feed (RD9) shows that with a set point of 85 K the cryocooler loses control of the cold finger temperature when the environment temperature goes above roughly 298 K (25 °C). The cryocooler performance curve from RD10 suggests the available heat lift on the cryocooler at this set point should be 19 W.

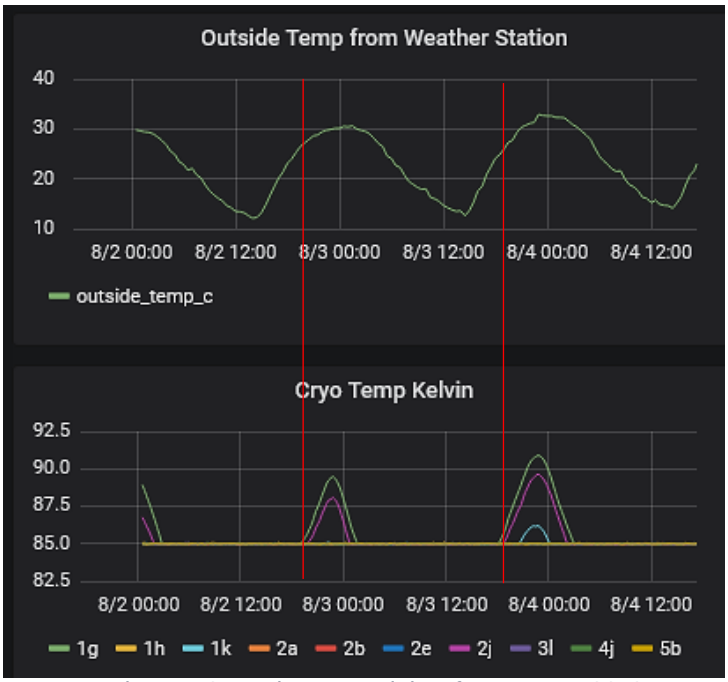

Figure 5-2 Feed measured data from August 2019

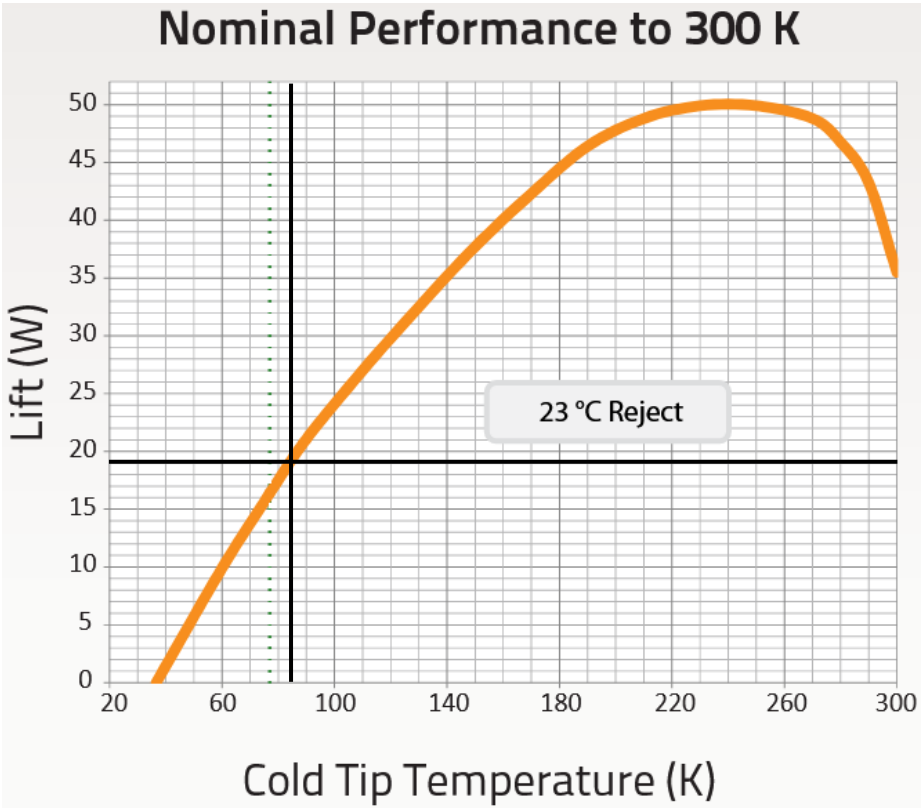

Figure 5-3 Cryocooler performance curve @ 23°C (296K) rejection environment from RD10

5.1 Results

The model predicted temperatures and heat load on the cryocooler are shown in Table 5-1 and Figure 5-4.

Component	Temperature (K)	Temperature Δ from set point (K)
Environment	298.0	-
Cold Finger	85.0	0.0
Feed baseplate (average)	98.3	13.3
Central Pyramid (base)	97.9	12.9
Central Pyramid (tip)	100.8	15.8
Arms (base)	100.9	15.9
Arms (tip)	154.3	69.3
Baseplate (average)	290.7	-
Radome (average)	291.2	-
Enclosure (average)	292.2	-
Heat load on cryocooler (W)	19.03	

Table 5-1 Analysis results of current design @ 85K setpoint and 298K environment temperature

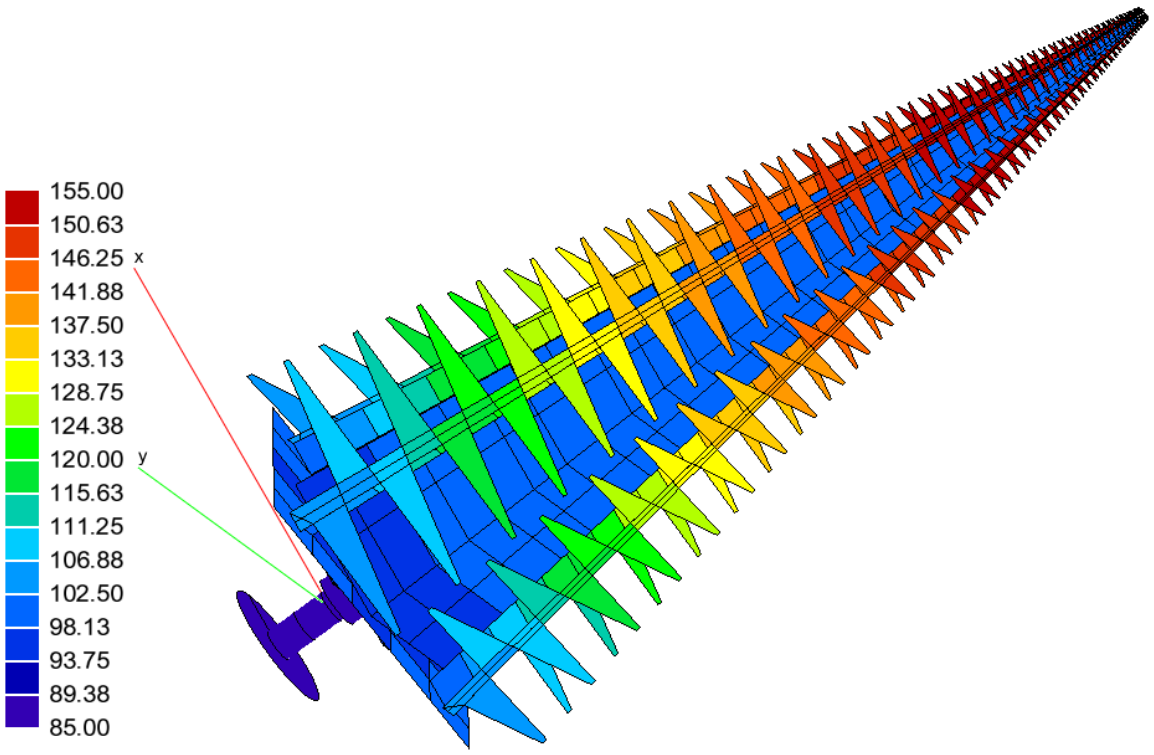

Figure 5-4 Temperature map of current design @ 85K setpoint and 298K environment temperature

The model is predicting a heat load on the cryocooler of 19.03 W with an environment temperature of 298 K, which matches with the behaviour seen in the cryocooler as it is currently running. The model is therefore predicting the reality of the current design very closely, assuming the cryocooler is operating at it's nominal performance seen in Figure 5-3. There is an inherent uncertainty in the thermal model results due to the use of the assumptions detailed in Section 4, however this correlation of the heat loads between the

model and the expected nominal cryocooler performance gives confidence in the veracity of the results.

5.2 Conclusions of Analysis

There are three notable conclusions that can be drawn from this analysis:

1. There is a large heat load on the cryocooler, which implies there is a large heat leak in the system
    - The radiative heat leak due to the emissivity of the copper is investigated in Section 6
    - The conductive heat leak through the titanium standoffs is investigated in Section 7

2. There is a ≈13 K gradient across the thermal strap from the cold finger to the feed baseplate, implying the thermal strap could be further optimised. This is investigated in Section 8

3. A large temperature gradient is seen up the length of the arms (≈69 K)
    - Reducing the radiative heat load on the arms will inherently reduce the temperature gradient (see Section 6)
    - The central pyramid walls are ≈4 times thicker than the arms and see a much reduced gradient, implying that thickening the material of the arms could reduce the gradient. This is investigated in Section 9.

6 Feed Emissivity Investigation

In order to investigate the effect of the feed emissivity, the emissivity of the copper surfaces was varied from 0.13-0.02 to represent a number of different surface finishes. The predicted temperatures and heat load on the cryocooler for each finish is shown in Table 6-1. The evolution of the total heat load on the cryocooler and arm tip temperature against feed emissivity is shown in Figure 6-1.

Component	Temperature (K)				
	Baseline ε=0.13	Oxidised copper ε=0.1	Un-oxidised bare copper ε=0.04 (RD3)	Gold electroplated ε=0.03 (RD3)	Gold vapour deposited ε=0.02 (RD3)
Environment	298.0				
Cold Finger	85.0				
Feed baseplate (average)	98.3	95.8	90.2	89.2	88.1
Central Pyramid (base)	97.9	95.5	90.1	89.1	88.0
Central Pyramid (tip)	100.8	97.7	91.0	89.8	88.6
Arms (base)	100.9	97.8	91.1	89.9	88.7
Arms (tip)	154.3	140.3	108.9	103.3	97.6
Baseplate (average)	290.7	291.1	292.3	292.5	292.8
Radome (average)	291.2	291.6	292.6	292.9	293.1
Enclosure (average)	292.2	292.6	293.4	293.6	293.9
Heat load on cryocooler (W)	19.0	15.5	7.7	6.3	4.7

Table 6-1 Effect of feed emissivity @ 85K setpoint and 298K environment temperature

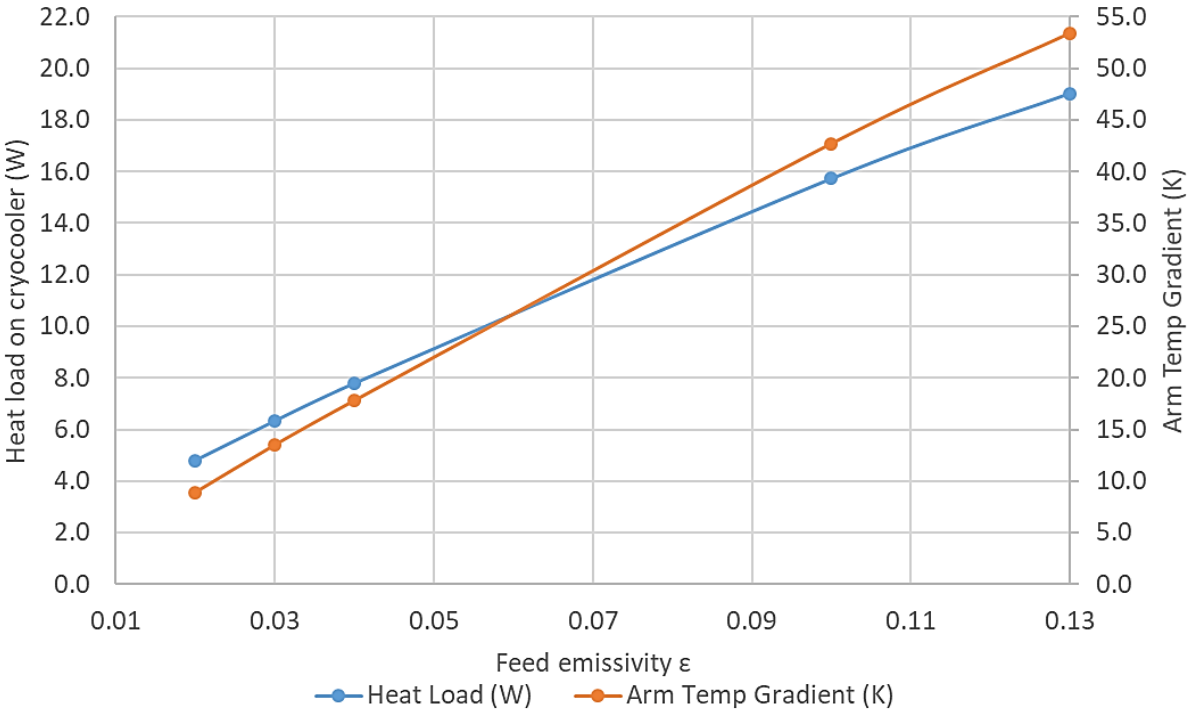

Figure 6-1 Effect of feed emissivity @ 85K setpoint and 298K environment temperature

It can be seen from the analysis results that the feed emissivity has a significant effect on the total heat load on the cryocooler. Gold plating the feed gives an at least 12.7 W reduction in the heat load, bringing it well within the 19 W limit. The knock-on effect of this reduction in radiative heat load is a large reduction in the temperature gradient up the arms, bringing the temperature at the tip of the arms to within 20 K of the set point temperature.

7 Stand-off Investigation

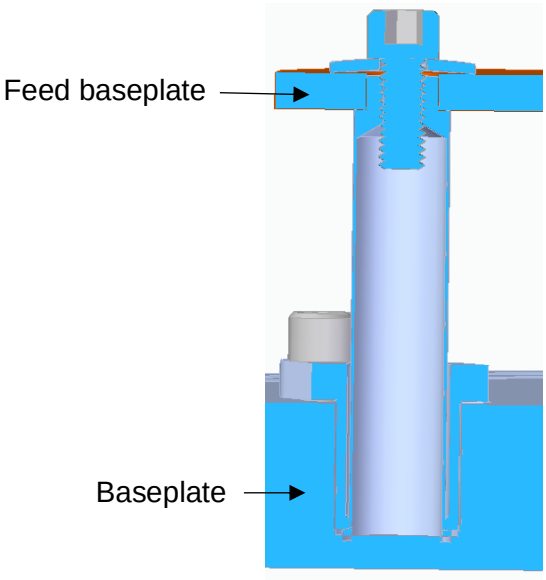

Figure 7-1 Titanium stand-offs

The current design includes 4 off titanium standoffs with the profile shown in Figure 7-1. This gives a conductive coupling of 0.00117 W/K per standoff. The analysis performed in Section 5 shows that this gives a temperature difference of 192.4 K across the standoffs. There is therefore a total heat leak through the stand-offs of 0.9 W. This conductive heat leak is negligible compared to the radiative heat leak demonstrated in Section 6 and is therefore not considered further.

8 Thermal Strap Investigation

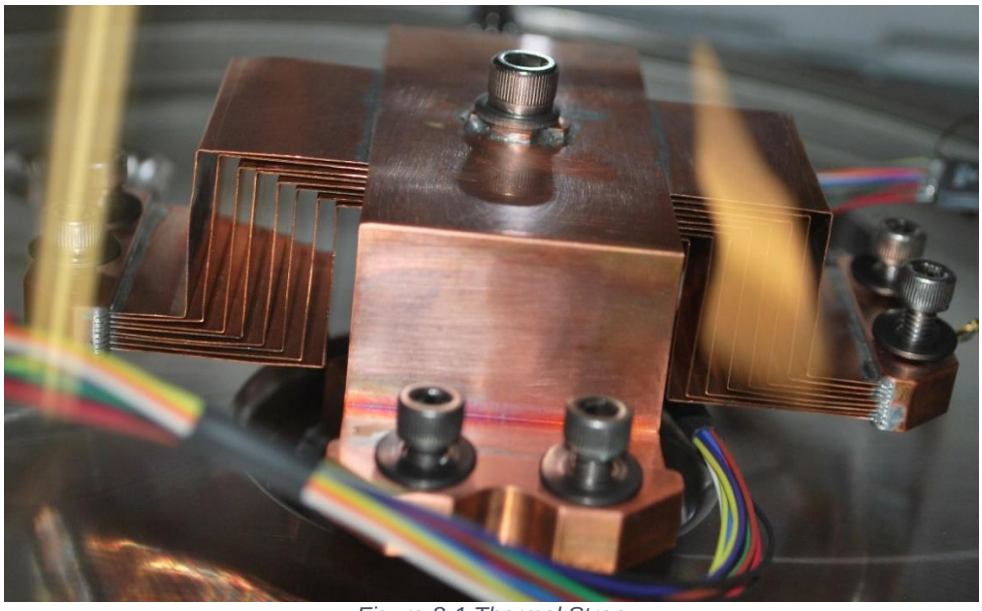

Figure 8-1 Thermal Strap

The current design of the thermal strap has a dry clamped interface between the strap and the cold finger, with 4 sets of 8 off 0.25 mm thick copper foils leading to dry bolted interfaces at the feed baseplate. This gives a total conductive coupling between the cold finger and the feed baseplate of 1.5 W/K.

This conductive coupling can be increased by using thermal grease at the interfaces to increase the contact conductance, or by increasing the thickness/number of the copper foils to increase the through strap conductance. The effect of these changes are shown in Table 8-1 and Figure 8-2.

Component	Temperature (K)			
	Baseline K = 1.5 W/K	Greased Interfaces K = 1.8 W/K	Greased & x2 foil thickness K = 3.4 W/K	Greased & x3 foil thickness K = 4.7 W/K
Environment	298.0			
Cold Finger	85.0			
Feed baseplate (average)	98.3	95.9	91.2	89.7
Central Pyramid (base)	97.9	95.6	90.9	89.3
Central Pyramid (tip)	100.8	98.4	93.7	92.1
Arms (base)	100.9	98.5	93.8	92.2
Arms (tip)	154.3	151.9	147.2	145.6
Baseplate (average)	290.7	290.7	290.6	290.5
Radome (average)	291.2	291.2	291.1	291.1
Enclosure (average)	292.2	292.2	292.1	292.1
Heat load on cryocooler (W)	19.0	18.7	18.8	18.8

Table 8-1 Effect of thermal strap @ 85K setpoint and 298K environment temperature

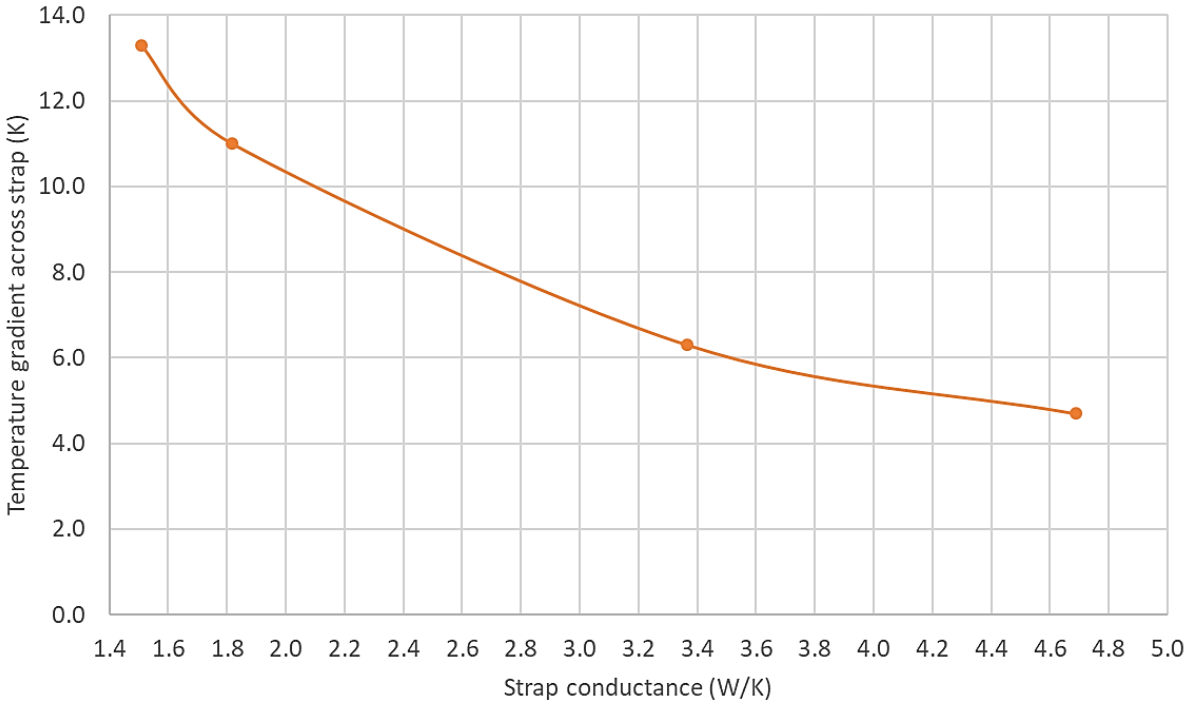

Figure 8-2 Effect of thermal strap @ 85K setpoint and 298K environment

It can be seen from Table 8-1 that the effect on the heat load is negligible, however there is a small but noticeable effect on the arm tip temperature due to the reduction in the temperature gradient across the thermal strap.

Greasing the interfaces has only a small effect, but when combined with doubling the foil thickness it more than halves the temperature gradient across the strap, causing a corresponding drop in arm tip temperature. Increasing the thickness past this point starts to have diminishing returns.

9 Arm Thickness Investigation

The feed arms are currently 0.76mm thick, which limits the conductive heat transfer up the length of the arms, driving large temperature gradients. The effect of increasing the thickness of the arms is shown in Table 9-1 and Figure 9-1.

Component	Temperature (K)			
	Baseline 0.76 mm	1 mm thickness	1.5 mm thickness	2 mm thickness
Environment	298.0			
Cold Finger	85.0			
Feed baseplate (average)	98.3	98.3	98.4	98.5
Central Pyramid (base)	97.9	97.9	98.0	98.1
Central Pyramid (tip)	100.8	100.8	100.8	100.9
Arms (base)	100.9	100.9	100.9	101.0
Arms (tip)	154.3	142.3	129.0	122.5
Baseplate (average)	290.7	290.7	290.7	290.7
Radome (average)	291.2	291.2	291.2	291.3
Enclosure (average)	292.2	292.2	292.2	292.2
Heat load on cryocooler (W)	19.03	19.1	19.2	19.8

Table 9-1 Effect of arm thickness @ 85K setpoint and 298K environment

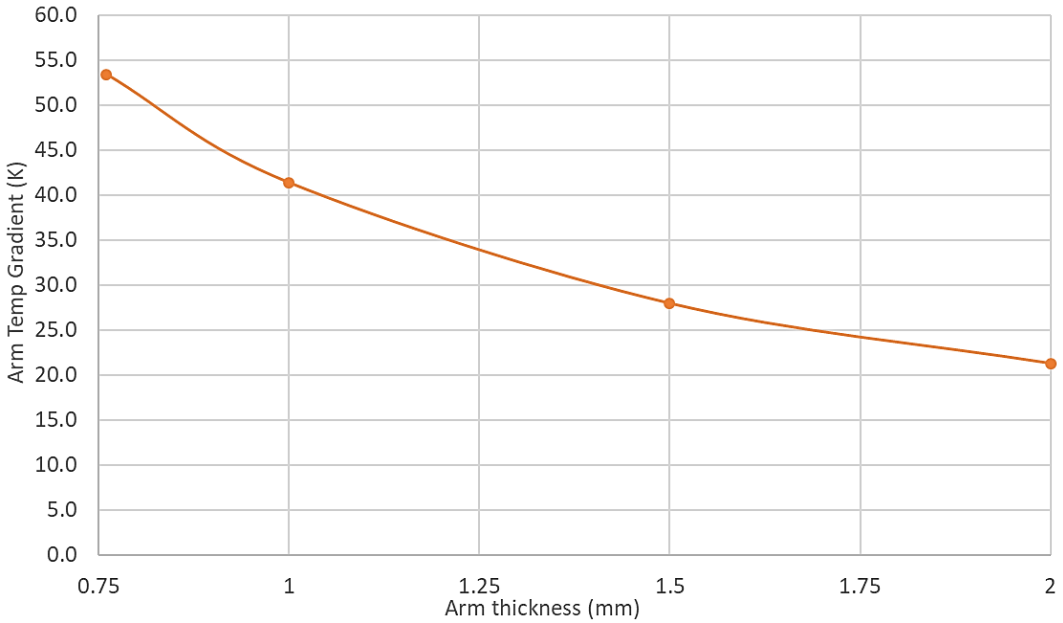

Figure 9-1 Effect of arm thickness @ 85K setpoint and 298K environment

Table 9-1 shows that by itself, increasing the thickness of the arms has a slight negative effect on the heat load on the cryocooler. However the positive effect on the temperature gradient up the arms is significant, and up to a thickness of 1.5mm outweighs the effect on the heat load. Past 1.5mm the positive effect on the gradient starts to reduce and the relative negative effect on the heat load starts to increase.

10 Conclusions and Recommendations

From the investigations detailed in the previous sections it can be seen that the emissivity of the copper has the largest effect on cryocooler heat load and feed performance. Gold plating the copper surfaces is predicted to reduce the heat load to well within the cryocoolers available heat lift, and bring the entirety of the feed assembly within 20K of the set point.

Further incremental improvements to the arm tip temperatures are available if necessary by:

- Use of thermal grease at the thermal strap interfaces
- Increasing the thickness of the strap foils by up to two times
- Increasing the thickness of the arms up to 1.5mm

The individual and cumulative effect of these changes on the cryocooler heat load and arm tip temperature across the desired set point range is shown in Figure 10-1 and Figure 10-2 respectively.

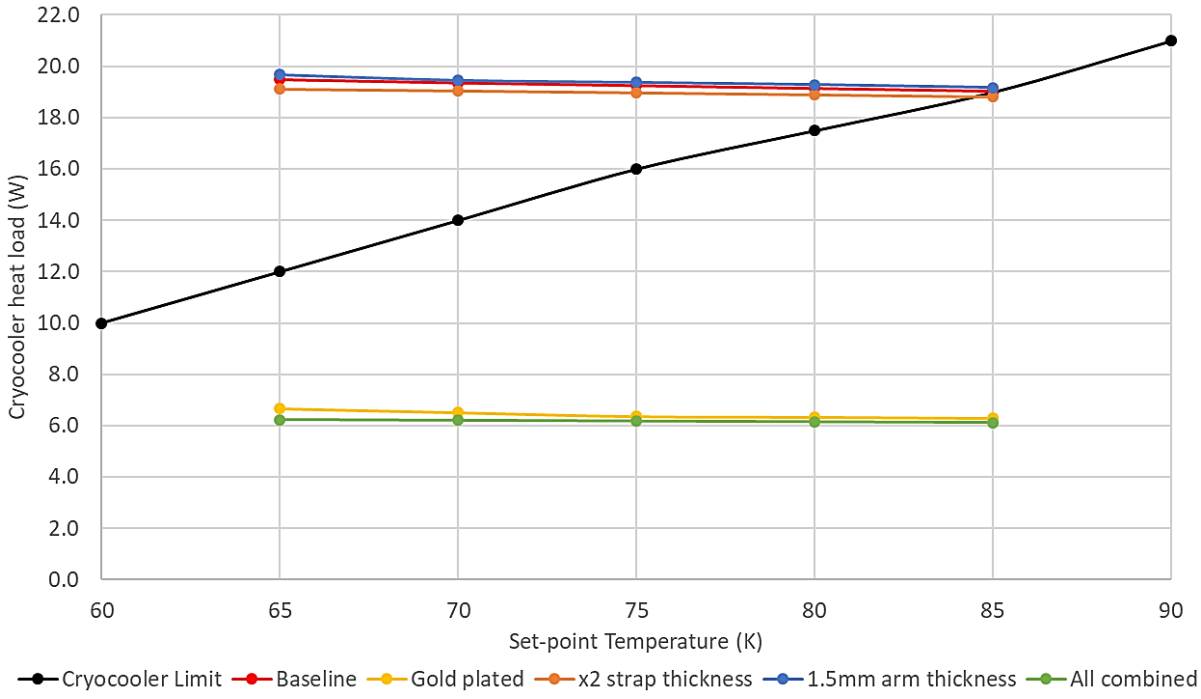

Figure 10-1 Heat load on cryocooler @ 65K-85K setpoints and 298K environment

Figure 10-1 includes the cryocooler available heat lift across this set point range according to the nominal performance curve shown in Figure 5-3. All datapoints above this line on the graph will therefore result in the cryocooler being unable to adequately control to the set point with the environment at 298K or above. It can be seen that gold plating is the only design update that will bring the heat load under the nominal cryocooler available heat lift across the entire desired set point range.

Figure 10-2 shows that gold plating has the largest individual effect on the maximum feed temperature, experienced at the tip of the arms. A further 8K improvement can be affected if necessary by the updates to the strap and arm thickness.

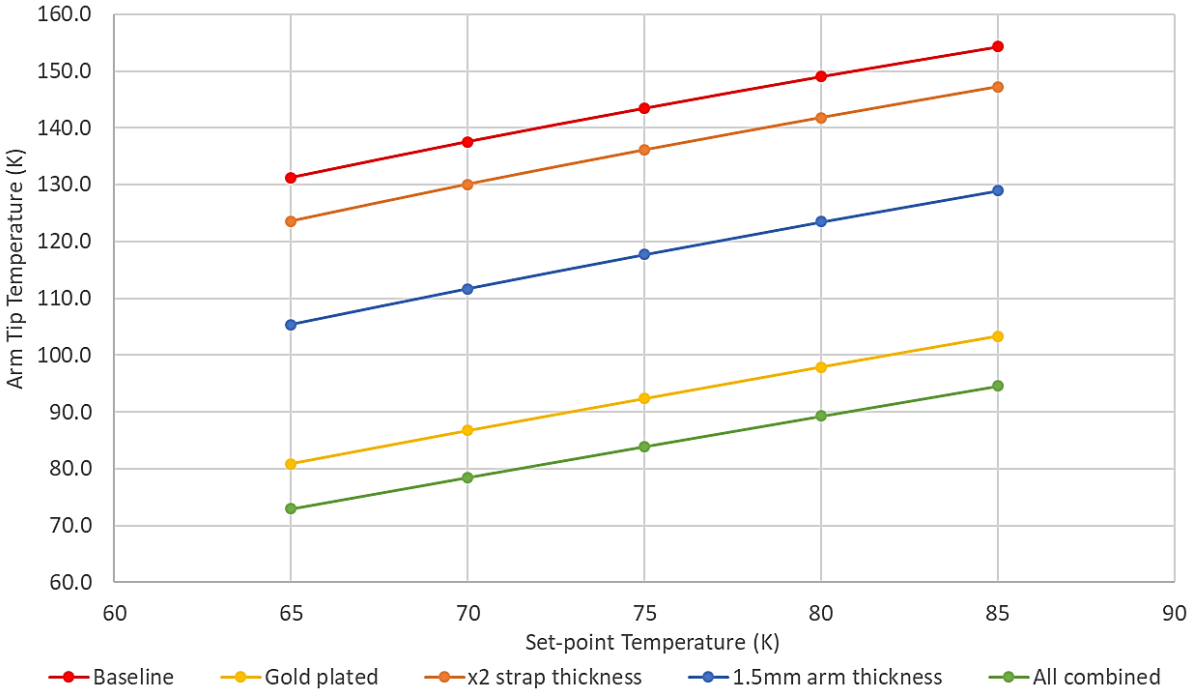

Figure 10-2 Arm tip temperature @ 65K-85K setpoints and 298K environment

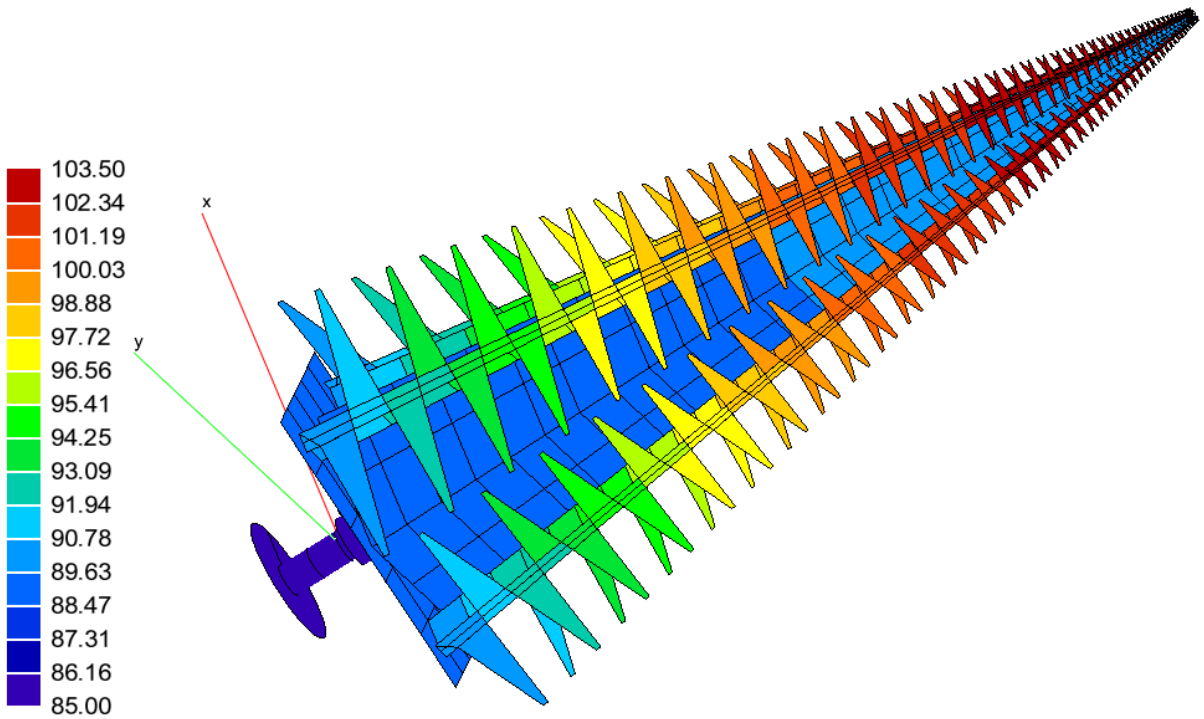

Figure 10-3 Temperature map of gold plated feed @ 85 K setpoint and 298K environment